Magnetic field norm SLAM using Gaussian process regression in foot-mounted sensors

Frida Viset*, Jan Tommy Gravdahl†, and Manon Kok*

***Abstract*— We propose an application of magnetic field norm simultaneous localisation and mapping to measurements from a foot-mounted sensor for pedestrian navigation. The algorithm is, to the best of the authors' knowledge, the first three dimensional drift-compensating indoor navigation method using only accelerometer, gyroscope and magnetometer measurements that does not rely on assumptions about the spatial structure of the indoor environment. We use a Rao-Blackwellized particle filter to simultaneously and recursively estimate the magnetic field norm map using reduced rank Gaussian process regression, and the position and orientation of the sensor. Our experiments demonstrate that our algorithm results in a drift-free position estimate using measurements collected from a foot-mounted sensor while walking around inside a hallway.**

I. Introduction

Precise indoor navigation using only body-worn sensors can be used in emergency response scenarios [1], in healthcare [2], and in commercial applications such as shopping malls and virtual reality gaming [3]. Navigation using only body-worn accelerometers and gyroscopes suffers from integration drift [4]. Outdoors, drift-free position estimates can be achieved when accelerometer and gyroscope measurements are combined with global navigation satellite system (GNSS) signals [5]. Indoors, GNSS signals are typically not available [1], [2], [3]. One way to limit the drift is to use a foot-mounted sensor, to detect the stance phase of the foot and use this to improve the position, velocity, and orientation estimates [6]. We remove the remaining drift using measurements from foot-mounted sensors by taking advantage of the rich spatial variations in the indoor magnetic field norm [7], by simultaneously navigation and mapping (SLAM) with the magnetic field norm anomalies.

A foot-mounted combined tri-axis gyroscope and accelerometer have previously been used to obtain accurate position estimates using the zero velocity update-aided extended Kalman filter (ZUPT-aided EKF), proposed by [6]. A tri-axis accelerometer, gyroscope and magnetometer can be integrated into the shoe of substantial footwear [8]. Our proposed algorithm builds on the open-source implementation of a ZUPT-aided EKF in [8]. The position estimate from a ZUPT-aided EKF is accurate for indoor position estimation on a shorter time scale. Still, over time, integration of velocity estimation errors causes the position estimation error to increase [9].

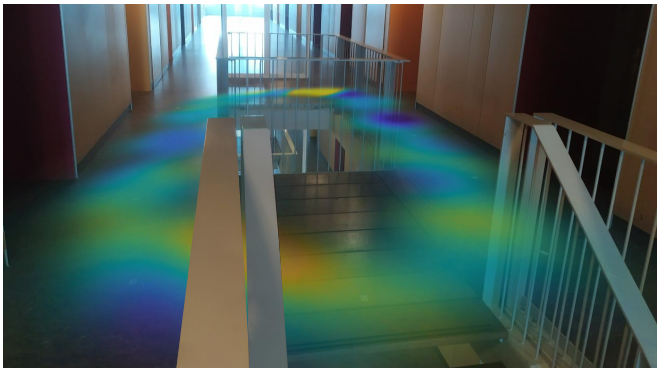

Fig. 1. Estimated magnetic field norm indoors from measurements from foot-mounted sensor.

Magnetic field SLAM has previously been used to achieve drift-free position estimates in two dimensions, by combining odometry from a foot-mounted sensor with magnetic field measurements [10]. Magnetic field SLAM using Gaussian process regression has been demonstrated to give drift-free position estimates using magnetic field measurements and encoder measurements from a cleaning robot [11]. Gaussian process regression scales in computational complexity with the number of input points [12]. Reduced-rank Gaussian process regression is a feasible and computationally tractable strategy for magnetic field mapping in indoor environments [13]. Computationally tractable Magnetic field SLAM using reduced-rank Gaussian process regression in a Rao-Blackwellized particle filter was proposed by [14] and used for on-board magnetic field measurements to compensate for position estimation drift in three dimensions. While the method proposed by [10] is limited to only two dimensions, the method proposed by [14] is not but relies on measurements from a camera in a hand-held smartphone in addition to the accelerometer and a gyroscope.

The contributions of this paper are twofold. Firstly, we propose an algorithm for online indoor localisation using only a foot-mounted tri-axis gyroscope, accelerometer and magnetometer using magnetic field norm SLAM. Secondly, we illustrate the benefit of the algorithm over existing methods by estimating the position of a pedestrian in the hallway depicted in Fig. 1. To the best of the author's knowledge, this is the first indoor pedestrian navigation algorithm

*Manon Kok and Frida Viset are with the Delft Center for Systems and Control, Delft University of Technology, the Netherlands. f.m.viset@tudelft.nl, M.Kok-1@tudelft.nl

†Jan Tommy Gravdahl is with the Department of Engineering Cybernetics, Norwegian University of Technology, the Netherlands. Jan Tommy Gravdahl acknowledges the funding of the Research Council of Norway through the IKTPLUSS funding scheme, project no. 304667, AROS. jan.tommy.gravdahl@ntnu.no. This work is part of the research programme "Sensor Fusion For Indoor Localisation Using The Magnetic Field" with project number 18213, which is (partly) financed by the Dutch Research Council (NWO).

that uses only a body-worn gyroscope, accelerometer and magnetometer, that compensates for drift upon revisitation of previously visited areas, that allows for three dimensional position estimation, and that does not rely on prior map information. We use similar assumptions that were used by [9] to model the sensors' motion and stance phases and a similar method for magnetic field mapping that was proposed by [14]. We formulate a joint state-space model for the simultaneous estimation of the foot-mounted sensors' position, velocity orientation and the magnetic field map. Our filter is accurate for short trajectories in a comparable way to the filter implemented by [9]. It compensates for drift in longer trajectories by recognising patterns in the magnetic field anomalies in a comparable way to the filter implemented by [14]. Our proposed algorithm finds a position estimate in three dimensions and achieves similar accuracy as [10] achieves in two dimensions.

The remainder of this paper is organised in the following way: Section II defines the estimation problem. Section III describes the sensor and kinematic models that constitute the dynamic model. Section IV describes the magnetic field and pseudo-zero velocity models that constitute the measurement model. Section V presents the resulting algorithm. Section VI shows the results of running our algorithm on an example set of measurements, and section VII summarises the results and discusses some possible directions for future research.

II. Problem formulation

Our focus is on estimating the position, velocity and orientation of a foot-mounted tri-axis gyroscope, accelerometer and magnetometer. The sensors' position and orientation are defined respectively as the translation and rotation from a world frame w to a sensor frame s. The velocity is defined as the time derivative of the position. The position p^{w} and velocity v^{w} are both vectors in $\mathbb{R}^3$, while the orientation is parametrised as a unit quaternion $q^{\mathrm{ws}} \in \mathbb{R}^4$ s.t. $\|q^{\mathrm{ws}}\|_2 = 1$.

The sensor frame is attached to the foot-mounted sensors, with the origin at the sensors' centre of mass, and with the axes aligned with the tri-axis gyroscope and accelerometer. The world frame is defined as a stationary frame with respect to the earth, which without loss of generality, has origin equal to the sensor frames' origin at time $t = 0$, has zero yaw angle displacement relative to the sensor frames' orientation at time $t = 0$, and whose z-axis is aligned with the local gravitational acceleration. We assume that Coriolis acceleration can be neglected in our model, as the magnitude of the Coriolis acceleration is below $3.39 \cdot 10^{-2}(\mathrm{m/s^2})$, which is smaller than the accelerometer measurement noise we use in our algorithm.

We estimate the posterior density $p(x_{1:t} \mid y_{1:t})$,

$$x_t = \begin{bmatrix} p_t^{\mathrm{w}} & v_t^{\mathrm{w}} & q_t^{\mathrm{ws}} & m_t \end{bmatrix}^{\mathsf{T}}, \tag{1}$$

$$y_t = \begin{bmatrix} y_{\mathrm{gyr},t}^{\mathrm{s}} & y_{\mathrm{acc},t}^{\mathrm{s}} & y_{\mathrm{mag},t} & y_{\mathrm{v},t}^{\mathrm{w}} \end{bmatrix}^{\mathsf{T}}, \tag{2}$$

where m_t denotes a vector encoding the magnetic field map, $y_{\mathrm{mag},t}$ is the magnetic field norm measurement, $y_{\mathrm{acc},t}^{\mathrm{s}}$ is the accelerometer measurement, $y_{\mathrm{gyr},t}^{\mathrm{s}}$ is the gyroscope measurement, $y_{\mathrm{v},t}^{\mathrm{w}}$ is a pseudo-measurement generated by a zero-velocity detection method [6], and where the notation $y_{1:t}$ refers to the set of vectors $\{y_1, \ldots, y_t\}$. We estimate the posterior density recursively. At each time step, we compute the current probability density estimate $\hat{p}(x_{1:t} \mid y_{1:t})$ given only the previous probability density estimate $\hat{p}(x_{1:t-1} \mid y_{1:t-1})$ and the incoming measurements y_t. We perform the recursive estimation in two steps: A dynamic update, and a measurement update. The dynamic update estimate the prior probability density

$$p(x_{1:t} \mid y_{\mathrm{acc},1:t}^{\mathrm{s}}, y_{\mathrm{gyr},1:t}^{\mathrm{s}}, y_{\mathrm{mag},1:t-1}^{\mathrm{s}}, y_{\mathrm{v},1:t-1}^{\mathrm{w}}), \tag{3}$$

using an estimate of the previous posterior probability density $p(x_{1:t-1} \mid y_{1:t-1})$, and the accelerometer and gyroscope measurements at time t. The measurement update estimates the posterior density $p(x_{1:t} \mid y_{1:t})$ using the estimate of the prior density.

III. Dynamic models

We model the gyroscope measurements as the angular velocity in sensor frame affected by white noise according to

$$y_{\mathrm{gyr},t}^{\mathrm{s}} = \omega_t^{\mathrm{s}} + e_{\mathrm{gyr},t}^{\mathrm{s}}, \qquad e_{\mathrm{gyr},t}^{\mathrm{s}} \sim \mathcal{N}(0, \sigma_{\mathrm{gyr}}^2 \mathcal{I}_3), \tag{4}$$

where ω_t^{s} is the sensors' angular velocity, $e_{\mathrm{gyr},t}^{\mathrm{s}}$ is the measurement noise, and σ_{gyr}^2 is assumed to be a known variance. Similarly, we model the acceleration measurement as the sensors' acceleration in the sensor frame affected by gravity and white noise according to

$$y_{\mathrm{acc},t}^{\mathrm{s}} = a_t^{\mathrm{s}} + g_t^{\mathrm{s}} + e_{\mathrm{acc},t}^{\mathrm{s}}, \qquad e_{\mathrm{acc},t}^{\mathrm{s}} \sim \mathcal{N}(0, \sigma_{\mathrm{acc}}^2 \mathcal{I}_3), \tag{5}$$

where a_t^{s} is the sensors acceleration, g^{s} is the gravity vector in sensor frame, $e_{\mathrm{acc},t}^{\mathrm{s}}$ is the white noise process corrupting the acceleration measurement, and σ_{acc}^2 is assumed to be a known variance.

The change in orientation given gyroscope measurements can be modelled recursively [15] for each timestep t as

$$q_t^{\mathrm{ws}} = q_{t-1}^{\mathrm{ws}} \odot \exp_{\mathrm{q}}\left(\tfrac{T}{2}(y_{\mathrm{gyr},t}^{\mathrm{s}} - e_{\mathrm{gyr},t}^{\mathrm{s}})\right), \tag{6}$$

where $\odot$ denotes the quaternion product, and $\exp_{\mathrm{q}}(\cdot)$ maps an orientation on axis-angle form to a quaternion (see [15] for details on quaternion algebra). The acceleration of the sensor can be found by subtracting the gravitational acceleration and the noise from the measured acceleration, according to

$$a_t^{\mathrm{w}} = R(q_t^{\mathrm{ws}})(y_{\mathrm{acc},t}^{\mathrm{s}} - e_{\mathrm{acc},t}^{\mathrm{s}}) - g^{\mathrm{w}}, \tag{7}$$

where $R(\cdot)$ is an operator transforming a unit quaternion to a rotation [16]. The position and velocity can then be described by the first-order Taylor approximation of the first and second discrete integral of acceleration

$$v_t^{\mathrm{w}} = v_{t-1}^{\mathrm{w}} + T a_t^{\mathrm{w}}, \tag{8}$$

$$p_t^{\mathrm{w}} = p_{t-1}^{\mathrm{w}} + T v_t^{\mathrm{w}}, \tag{9}$$

where T is the timestep of the discrete-time approximation.

IV. Measurement models

Similar to [8], we detect the stance phase of the step by investigating when the function

$$\begin{aligned} &D(y^{\text{s}}_{\text{acc},t-W-1:t}, y^{\text{s}}_{\text{gyr},t-W-1:t}) \\ &= \tfrac{1}{W} \sum_{k=t-W-1}^{t} \left(\tfrac{1}{\sigma^2_{\text{acc}}} \left\| y^{\text{s}}_{\text{acc},k} - g \tfrac{\bar{y}^{\text{s}}_{\text{acc},t-W-1:t}}{\left\| \bar{y}^{\text{s}}_{\text{acc},t-W-1:t} \right\|_2} \right\|_2^2 \right. \\ &\left. + \tfrac{1}{\sigma^2_{\text{gyr}}} \left\| y^{\text{s}}_{\text{gyr},k} \right\|_2^2 \right) \end{aligned} \tag{10}$$

is below a threshold γ [17]. The gravitational acceleration magnitude is denoted g, where $\bar{y}_{t:t'}$ denotes the average of the set of vectors $y_t, \ldots, y_{t'}$, $\| \cdot \|_2$ denotes the 2-norm, and W is a tunable detection window [17]. We model the information from the zero-velocity detector similarly to [6] as a pseudo-measurement of the velocity

$$y^{\text{w}}_{\text{v},t} = 0_{3\times 1} = v^{\text{w}}_t + e^{\text{w}}_{\text{v},t}, \qquad e^{\text{w}}_{\text{v},t} \sim \mathcal{N}(0, \sigma^2_{\text{v}} \mathcal{I}_3), \tag{11}$$

where $e^{\text{w}}_{\text{v},t}$ is pseudo-measurement noise, and σ^2_{v} is a tunable parameter. The measurement is assumed to be given by this model every time the zero-velocity detector is active [6], and when it is inactive, we assume that the zero-velocity pseudo measurement is not available, and model it as an empty set.

A tri-axis magnetometer measures the magnetic field. We assume the magnetic field norm measurement is normally distributed about the true magnetic field norm in the position of the measurement, according to

$$y_{\text{mag},t} = \left\| H(p^{\text{w}}_t) \right\|_2 + e_{\text{mag},t}, \qquad e_{\text{mag},t} \sim \mathcal{N}(0, \sigma^2_{\text{mag}}) \tag{12}$$

where $H(p^{\text{w}}_t)$ is the magnetic field in the sensor position at time t, $y_{\text{mag},t}$ is the norm of the tri-axis magnetic field measurement $y^{\text{s}}_{\text{mag},t}$, and $e_{\text{mag},t}$ is the magnetometer measurement noise.

We consider the magnetic field norm to be a nonlinear function $\left\| H(p) \right\|_2 : \mathbb{R}^3 \to \mathbb{R}$, mapping the position p to a magnetic field norm. We model the nonlinear function using a Gaussian process prior

$$\left\| H(p) \right\|_2 \sim \mathcal{N}(0, \kappa_{\text{SE}}(\cdot, \cdot)), \tag{13}$$

with a squared exponential kernel

$$\kappa_{\text{SE}}(p, p') = \sigma^2_{\text{SE}} \exp \tfrac{-\left\| p - p' \right\|_2^2}{2 l^2_{\text{SE}}}, \tag{14}$$

to include the assumption that the magnetic field norm is similar in nearby locations, and variations typically have the magnitude σ_{SE} and length-scale l_{SE} [14].

Recursive reduced-rank Gaussian process regression using Hilbert-space methods can be used to estimate the magnetic field norm as a scaled sum of basis functions in a finite domain [18]. The basis functions are defined as solutions to the negative Laplace equations that is subject to the Dirichlet boundary condition [18]. The basis functions are denoted $\phi_k : \mathbb{R}^3 \to \mathbb{R}$, and the negative Laplace equations subject to the Dirichlet boundary conditions are

$$\begin{cases} -\nabla^2 \phi_k(p^{\text{w}}) = \lambda_k \phi_k(p^{\text{w}}), & p^{\text{w}} \in \Omega, \\ \phi_k(p^{\text{w}}) = 0, & p^{\text{w}} \in \partial\Omega, \end{cases} \tag{15}$$

with λ_k denoting the eigenvalues over a closed and connected domain $\Omega \subset \mathbb{R}^3$ with edge $\partial\Omega$.

The Gaussian process regression d-step ahead prediction in a position p^{w}_t can be approximated using a linear combination of the N_{m} first basis functions according to

$$\hat{p}(y_{\text{mag},t} | p^{\text{w}}_t, \widehat{m}_{t-d}) = \mathcal{N}(\mu_{\text{mag},t|t-d}, S_{t|t-d}) \tag{16a}$$

$$\mu_{\text{mag},t|t-d} = \Phi(p^{\text{w}}_t) \widehat{m}_{t-d} \tag{16b}$$

$$S_{t|t-d} = \Phi(p^{\text{w}}_t) P_{\text{m},t-d} \Phi(p^{\text{w}}_t)^{\mathsf{T}} + \sigma^2_{\text{mag}}, \tag{16c}$$

where $d \geq 1$ denotes a delay, and where $\widehat{m}_{t-d}$ and $P_{\text{m},t-d}$ are computed recursively using all available measurements up until time $t - d$, according to

$$S_{t|t-1} = \Phi(p^{\text{w}}_t) P_{\text{m},t-1} \Phi(p^{\text{w}}_t)^{\mathsf{T}} + \sigma^2_{\text{mag}}, \tag{17a}$$

$$K_{t|t-1} = P_{\text{m},t-1} \Phi(p^{\text{w}}_t)^{\mathsf{T}} S^{-1}_{t|t-1}, \tag{17b}$$

$$m_t = m_{t-1} + K_{t|t-1}(y_{\text{m},t} - \Phi(p^{\text{w}}_t) m_{t-1}), \tag{17c}$$

$$P_{\text{m},t} = P_{\text{m},t-1} - K_{t|t-1} S_{t|t-1} K^{\mathsf{T}}_{t|t-1}, \tag{17d}$$

with $\Phi(p^{\text{w}}_t) = \begin{bmatrix} \phi_1(p^{\text{w}}_t) & \cdots & \phi_{N_{\text{m}}}(p^{\text{w}}_t) \end{bmatrix}$. The recursion is initialised with $\widehat{m}_0 = 0$, $P_{\text{m},0} = \Lambda$, with

$$\Lambda = \begin{bmatrix} S(\sqrt{\lambda_1}) & \cdots & 0 \\ \vdots & \ddots & \vdots \\ 0 & \cdots & S(\sqrt{\lambda_{N_{\text{m}}}}) \end{bmatrix}, \tag{18}$$

where the function $S(\sqrt{\lambda_k})$ is the spectral density [19] of the squared exponential kernel (14)

$$S_{\text{SE}}(\sqrt{\lambda_k}) = \sigma^2_{\text{SE}} \left(2\pi l^2_{\text{SE}} \right)^{\frac{3}{2}} \exp(-\tfrac{\lambda_k l^2_{\text{SE}}}{2}). \tag{19}$$

V. Estimation

The system model is defined by (6)–(9), (11) and (16b)–(16c). We consider this a nonlinear stochastic state-space model where $y^{\text{s}}_{\text{gyr},t}$ and $y^{\text{s}}_{\text{acc},t}$ are noisy inputs to the dynamic model, and where $y^{\text{w}}_{\text{v},t}$ and $y_{\text{mag},t}$ are measurements. The measurements $y^{\text{w}}_{\text{v},t}$ and $y_{\text{mag},t}$ are linear functions of the velocity and the magnetic field map vector. The measurement $y_{\text{mag},t}$ is, however, a nonlinear function of the position. Rao-Blackwellized particle filters estimate states that are a result of nonlinear state-space models with linear substructures. Since our model is nonlinear, with some linear and some almost linear substructures, we apply a Rao-Blackwellized particle filter to a model with linearized substructures. The model (6)–(8) is commonly linearised around the current estimate in order to apply the EKF to include the zero-velocity pseudo measurements [20]. The high accuracy of this approach [6] confirms that (6)–(8) can safely be approximated by linearisation. The state of a nonlinear stochastic process with a conditionally linear substructure can be estimated using a Rao-Blackwellized particle filter [21]. We take advantage of the approximately linear substructure of our state-space model to estimate the posterior probability density in (20) using a Rao-Blackwellized particle filter [22]. The Rao-Blackwellized particle filter splits the state vector into a conditionally linear and a nonlinear part. The nonlinear part is represented by particles, where each particle

is considered a sample of the posterior probability density. The linear part of each particle's state is estimated with a conditional Kalman filter, given the corresponding nonlinear part of the particle's state [22]. For the foot-mounted sensor, we consider both the linear and the nearly linear structures as linear substructures in the state-space model and estimate the magnetic field, the orientation and the velocity as conditionally linear states given the position of each particle. We factorise the posterior density as

$$\begin{aligned} &p(p^{\mathrm{w}}_{1:t}, v^{\mathrm{w}}_{1:t}, q^{\mathrm{ws}}_{1:t}, m_{1:t} \mid y_{1:t}) \\ &= p(p^{\mathrm{w}}_{1:t} \mid y_{1:t}) p(v^{\mathrm{w}}_{1:t}, q^{\mathrm{ws}}_{1:t} \mid y_{1:t}, p^{\mathrm{w}}_{1:t}) \\ &\quad p(m_{1:t} \mid y_{1:t}, p^{\mathrm{w}}_{1:t}, v^{\mathrm{w}}_{1:t}, q^{\mathrm{ws}}_{1:t}), \end{aligned} \tag{20}$$

and estimate the probability density $p(p^{\mathrm{w}}_{1:t} \mid y_{1:t})$ with a particle filter, and the probability density $p(v^{\mathrm{w}}_{1:t}, q^{\mathrm{ws}}_{1:t} \mid y_{1:t}, p^{\mathrm{w}}_{1:t})$ using a conditional EKF given the position trajectory of each particle, by taking advantage of the fact that the model is approximately linear about the velocity and orientation. The probability density $p(m_{1:t} \mid y_{1:t}, p^{\mathrm{w}}_{1:t}, v^{\mathrm{w}}_{1:t}, q^{\mathrm{ws}}_{1:t})$ we approximate with the probability density $p(m_{1:t} \mid y_{1:t}, p^{\mathrm{w}}_{1:t})$ because the measurement model of the magnetic field is independent of the sensors' velocity and orientation. The density $p(m_{1:t} \mid y_{1:t}, p^{\mathrm{w}}_{1:t})$ can then be estimated with a conditional Kalman filter, by taking advantage of the fact that the model is linear about the magnetic field vector.

The posterior density (20) is computed recursively using a RBPF as summarised in Algorithm 1. To update the orientation estimate, we parametrise the deviation between the true and estimated orientation on axis-angle form [23] according to

$$q^{\mathrm{ws}}_t = \exp_{\mathrm{q}}\left(\tfrac{\eta^{\mathrm{w}}_t}{2}\right) \odot \hat{q}^{\mathrm{ws}}_t, \tag{21}$$

where $\eta^{\mathrm{w}}_t \in \mathbb{R}^3$ denotes an orientation deviation state. The system is then linearised with respect to $\eta^{\mathrm{w}}_t \in \mathbb{R}^3$. Algorithm 1 initialises the posterior density estimate by setting the position of all particles to zero, which is a reflection of the fact that at $t = 0$, the displacement between the sensor and world frame is zero. It uses any incoming pseudo zero-velocity measurements to update the conditional velocity and orientation state of each particle using an EKF measurement update, defined as

$$K^i_t = P^i_{t|t-1} H^{\mathsf{T}}_t (\sigma^2_{\mathrm{v}} \mathcal{I}_3 + H_t P^i_{t|t-1} H^{\mathsf{T}}_t)^{-1}, \tag{22a}$$

$$\begin{bmatrix} \hat{v}^{\mathrm{w},i}_{t|t}, \\ \hat{\eta}^{\mathrm{w},i}_t \end{bmatrix} = \begin{bmatrix} \hat{v}^{\mathrm{w},i}_{t|t-1}, \\ 0_{3\times 1} \end{bmatrix} + K^i_t (y_{v,t} - \hat{v}^{\mathrm{w},i}_{t|t-1}), \tag{22b}$$

$$P^i_{t|t} = P^i_{t|t-1} - K^i_t H_t P^i_{t|t-1}, \tag{22c}$$

$$\hat{q}^{\mathrm{ws},i}_{t|t} = \exp_{\mathrm{q}}(\tfrac{\hat{\eta}^{\mathrm{w},i}_t}{2}) \odot \hat{q}^{\mathrm{ws},i}_{t|t-1}. \tag{22d}$$

This update is based on a linearisation of (6)–(8), and of (11), using the Jacobian $H_t = \begin{bmatrix} \mathcal{I}_3 & 0_{3\times 3} \end{bmatrix}$.

We then use the magnetic field measurement in the current position to evaluate the likelihood of each particle according to the weights

$$w^i_t = \hat{p}(y_{\mathrm{mag},t} \mid p^{\mathrm{w},i}_{t|t-1}, \widehat{m}^i_{t-d}, P^i_{\mathrm{m},t-d}) w^i_{t-1}, \tag{23}$$

with the probability density estimate defined in (16a)–(16c), and perform selective resampling with criterion $M_{\mathrm{eff}} < 2/3M$, where M is the number of particles, and M_{eff} is the effective number of particles (see [22]). The weights are normalised at each timestep so that $\sum_i^N w^i_t = 1$. As the re-sampled particle cloud are samples from the estimated posterior density $\hat{p}(p^{\mathrm{w}}_{1:t} \mid y_{1:t})$, we denote this step the particle filter measurement update. We perform a recursive update of the magnetic field norm map according to (17a)–(17d) in a Kalman filter measurement update. We then propagate the positions of our particles by simulating the linear state as an uncertain input, according to

$$\tilde{v}^{\mathrm{w},i}_t \sim \mathcal{N}(\hat{v}^{\mathrm{w},i}_{t|t}, H_t P^i_{t|t-1} H^{\mathsf{T}}_t), \tag{24a}$$

$$p^{\mathrm{w},i}_{t+1|t} = p^{\mathrm{w},i}_{t|t} + T \tilde{v}^{\mathrm{w},i}_t, \tag{24b}$$

where $\tilde{v}^{\mathrm{w},i}_t$ denotes the Monte-Carlo sampled velocity for particle i at time t. We denote this step the PF dynamic update, as it uses the information from the dynamic model to update the particles so they are samples from the estimated prior $\hat{p}(p^{\mathrm{w}}_{1:t+1} \mid y_{1:t})$. We use the new positions of each particle as a pseudo measurement of the linear states according to the dynamic equations. The update is defined as

$$K^i_t \leftarrow P^i_{t|t} H^{\mathsf{T}}_t T (T^2 H_t P^i_{t|t} H^{\mathsf{T}}_t)^{-1}, \tag{25a}$$

$$\begin{bmatrix} \hat{v}^{\mathrm{w},i}_{t|t} \\ \hat{\eta}^{\mathrm{w},i}_t \end{bmatrix} \leftarrow \begin{bmatrix} \hat{v}^{\mathrm{w},i}_{t|t} \\ 0_{3\times 1} \end{bmatrix} + K^i_t (p^{\mathrm{w},i}_{t+1|t} - p^{\mathrm{w},i}_{t|t} - T\hat{v}^{\mathrm{w},i}_{t|t}), \tag{25b}$$

$$\hat{q}^{\mathrm{ws},i}_{t|t} \leftarrow \exp_{\mathrm{q}}(\tfrac{\hat{\eta}^{\mathrm{w},i}_t}{2}) \odot \hat{q}^{\mathrm{ws},i}_{t|t}, \tag{25c}$$

$$P^i_{t|t} \leftarrow P^i_{t|t} - T K^i_t H_t P^i_{t|t}, \tag{25d}$$

with the arrow indicating that the values on the right side replace the values on the left. We denote this the EKF dynamic measurement update according to the convention in [22].

Finally, we perform an EKF dynamic update of the conditionally approximately linear states by letting

$$\hat{v}^{\mathrm{w},i}_{t+1|t} = \hat{v}^{\mathrm{w},i}_{t|t} + T(R(\hat{q}^{\mathrm{ws},i}_t) y^{\mathrm{s}}_{\mathrm{acc},t} - g^{\mathrm{w}}), \tag{26a}$$

$$\hat{\eta}^{\mathrm{w},i}_{t+1|t} = \hat{\eta}^{\mathrm{w},i}_{t|t}, \tag{26b}$$

$$P^i_{t+1|t} = F_t P^i_{t|t} F^{\mathsf{T}}_t + G^i_t \begin{bmatrix} \sigma^2_{\mathrm{acc},t} \mathcal{I}_3 & 0_{3\times 3} \\ 0_{3\times 3} & \sigma^2_{\mathrm{gyr},t} \mathcal{I}_3 \end{bmatrix} (G^i_t)^{\mathsf{T}}, \tag{26c}$$

using the Jacobians

$$F_t = \begin{bmatrix} \mathcal{I}_3 & T[y^{\mathrm{w}}_{\mathrm{acc},t}\times] \\ 0_{3\times 3} & \mathcal{I}_3 \end{bmatrix}, \tag{27}$$

$$G_t = \begin{bmatrix} TR(\hat{q}^{\mathrm{ws},i}_{t-1|t-1}) & 0_{3\times 3} \\ 0_{3\times 3} & -TR(\hat{q}^{\mathrm{ws},i}_{t-1|t-1}) \end{bmatrix}, \tag{28}$$

of the dynamic model (6)–(8), where $\hat{q}^{\mathrm{ws},i}_{t-1|t-1}$ is the orientation estimate of each particle, and $[y^{\mathrm{w}}_{\mathrm{acc},t}\times]$ is the scew-symmetric matrix representation of the vector $y^{\mathrm{w}}_{\mathrm{acc},t}$ [15].

In applying the Rao-Blackwellized particle filter as defined in [22] to the state-space model in (6)–(8) and the magnetic field norm measurement model, we made one modification.

The weights of the particles are only evaluated using the magnetic field measurement, not the pseudo-zero-velocity measurements. The zero-velocity pseudo measurements reduce the spread of the particle cloud, causing all the positions of the particles to be the same at the end of each footstep. This modification ensures that the spread of the particle cloud is large enough to discover revisitation of previous positions.

Fig. 2. Experimental setup with foot-mounted sensor.

Algorithm 1 Magnetic field norm SLAM for foot-mounted sensor

Input: $\{y_{\text{acc},t}, y_{\text{gyr},t}, y_{\text{m},t}\}_{t=1}^{N}$

Output: $\{p_{t|t}\}_{t=1}^{N}$

Initialisation: $p_{0|-1}^{\text{w},i} = 0_{3\times1}$, $\hat{v}_{0|-1}^{\text{w},i} = 0_{3\times1}$, $\hat{q}_{0|-1}^{\text{ws},i} = q_0^{\text{ws}}$, $P_{0|-1}^{i} = P_0$, $\widehat{m}_0^i = 0_{N_\text{m}\times1}$, $P_{\text{m},0}^{i} = \Lambda$, w_t^i

for $t = 1$ to N **do**
  if $(D(y_{\text{acc},(t-W-1):t}, y_{\text{gyr},(t-W-1):t}) < \gamma)$ **then**
    Extended Kalman filter measurement update according to (22a)- (22d).
  end if
  Particle filter measurement update according to (23). **if** $M_{\text{eff}} > \frac{2}{3}M$ **then** Resample, set $w_t^i = \frac{1}{M}$.
  Kalman filter measurement update given by (17a)–(17d).
  Particle filter dynamic update using $\tilde{v}_t^{\text{w},i}$, a Monte-Carlo sampled velocity according to (24a)-(24b).
  Extended Kalman filter dynamic measurement update according to (25a)-(25d).
  Extended Kalman filter dynamic update according to (26a)- (26c).
end for

VI. Experimental Results

Measurements were collected using an Xsens MTi 100 IMU at a frequency of 100Hz. Fig. 2 shows the experimental setup on a foot. We collected measurements while the test subject was walking around in circles in the hallway in Fig. 1. We marked checkpoints with tape on the floor in the indoor environment where the measurements were collected, as shown in Fig. 4. The test subject stepped only on the checkpoints while collecting the measurements. The root-mean-squared revisitation error of the position estimate was calculated at the marked checkpoints.

The domain Ω, used to define the basis functions in (15), is chosen as the smallest possible cuboid where each point is no closer than 2 meters of any position trajectory estimate to avoid boundary effects. We centred the magnetic field measurements by subtracting the mean magnetic field measurement of the full measurement sequence. The centred magnetic field norm measurements from the IMU in the indoor environment had variations with a magnitude of around 1, so we chose $\sigma_{\text{SE}}^2 = 1$. As the magnetic field anomalies tend to rapidly change along the z-direction close to the floor [24], we set the length-scale $l_{\text{SE}} = 0.3$ meters to accurately estimate the details of the magnetic field norm variations in the indoor environment. The measurement noise was set slightly higher than the sensors' magnetometer measurement noise of $\sigma_{\text{mag}} = 0.001$, to $\sigma_{\text{mag}} = 0.01$, to compensate for errors in the model. We choose to down-sample the magnetic field measurements to 10Hz to reduce the computational load. This measurement frequency is still high enough to map the magnetic field anomalies [14]. To investigate how many basis functions were necessary to approximate the GP prediction accurately, we sampled 200 simulated magnetic field measurements from the chosen GP prior and 100 simulated magnetic field test values in non-overlapping test positions. The prediction accuracy of the simulated magnetic field value in the test-positions was compared with the accuracy of the reduced-rank GP prediction in the same 100 test positions. The root-mean-squared prediction error in the test positions is displayed in Fig. 3 for a varied number of basis functions. The reduced-rank GP prediction converges to the true GP prediction at approximately 2000 basis functions, so N_m was chosen to be 2000.

Our position estimation results are compared with the position estimates from an open-source implementation of the ZUPT-aided EKF from [8] applied to the same measurements. As the sensor is front-mounted, we can expect the position estimate to drift more compared to what is reported for heel-mounted sensors [17]. The parameters for the ZUPT-aided EKF were chosen to give as good position estimates as possible given the test subjects' walking patterns. The accelerometer and gyroscope standard deviations were set to $\sigma_{\text{acc}} = 0.12\text{ms}^{-2}$ and $\sigma_{\text{gyr}} = 0.006°\text{s}^{-1}$, respectively. The threshold γ for the zero-velocity detector was set to $2 \cdot 10^7$, and the time window $W = 12$. The measurement noise of the velocity pseudo-measurement was set to $\sigma_\text{v} = 0.12$. The initial covariance for the position, velocity and orientation was set to $P_0 = 0.0012\mathcal{I}_9$. The strength of the local gravity field in Delft is $g = 9.81\text{ms}^{-2}$ [25]. For Algorithm 1, the zero-velocity parameters, the gyroscope and the accelerometer measurement noise were given the same values in the ZUPT-aided EKF. The initial velocity and orientation covariance in the proposed Algorithm 1 was set to $P_0 = 0.0012\mathcal{I}_6$, to reflect the initial covariance in the ZUPT-aided EKF. The delay was chosen as $d = 2$ seconds.

The results in Fig. 7 compares the revisitation errors

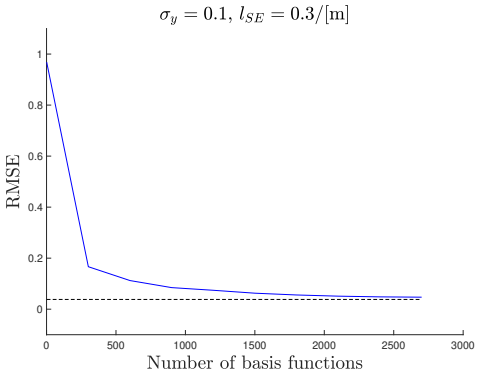

Fig. 3. The blue line shows the RMSE of the predicted magnetic field norm in of a reduced-rank GP prediction against the number of basis functions that was used to approximate the true GP prediction. The black dotted line shows the RMSE of the true GP prediction of the magnetic field norm.

between Algorithm 1 and the ZUPT-aided EKF from [8]. The two position estimates have similar accuracy at the beginning of the trajectory. Still, over time, the position estimate from Algorithm 1 does not drift away from the true position, unlike the position estimate obtained using the ZUPT-aided EKF from [8]. The RMSE position estimate at the checkpoints using the ZUPT-aided EKF is 1.68 meters, and using Algorithm 1 it is 0.16 meters.

The trajectory and magnetic field norm map of the current highest-weight particle is displayed for four different times in Fig. 5. The magnetic field estimation certainty is visibly higher near the checkpoints. This is because the checkpoints mark the location of the stance phase of the foot. In these locations, more magnetic field measurements are available, which gives a more confident prediction. The details of the magnetic field anomalies become more apparent when the area is visited multiple times, as can be seen, by comparing Fig. 5(a), that shows the magnetic field map estimate after one lap, with Fig. 5(d), that shows the magnetic field map at the end of the six laps around the 12 checkpoints. These results reflect how Gaussian process regression with a squared exponential kernel predicts the function value more confidently close to previous measurements [26]. The estimated magnetic field is visibly rich in spatial variation, which makes it possible for the particle filter to compensate for drift in the position estimate, as can be seen in Fig. 6. The figure compares the position trajectory for six laps around the marked checkpoints with the positions estimated with the ZUPT-aided EKF from [8] with the estimate using Algorithm 1.

VII. Conclusions and Future Work

The experimental results demonstrate how Algorithm 1 for foot-mounted sensors compensates for drift by recognising patterns in the magnetic field norm anomalies in previously visited positions. The results illustrate the removal of drift in a short trajectory in a fixed size domain.

It is worth mentioning that using 2000 basis functions to store the magnetic field in the particle filter is computationally demanding. This is because each of the M

Fig. 4. The twelve labelled checkpoints used for collecting measurements.

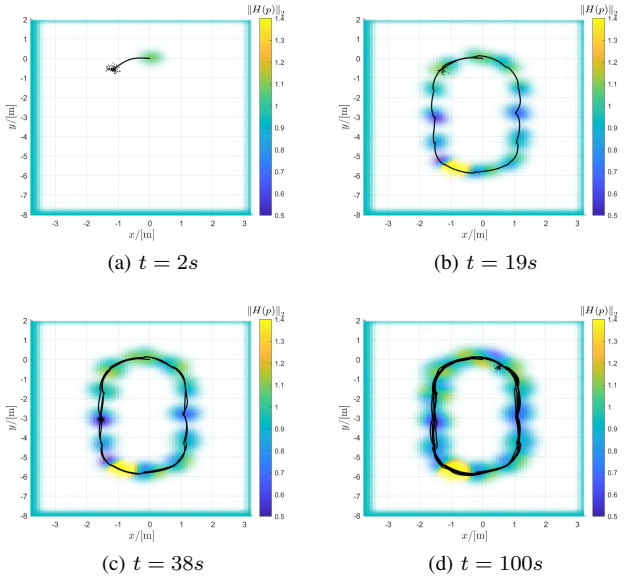

(a) $t = 2s$ (b) $t = 19s$

(c) $t = 38s$ (d) $t = 100s$

Fig. 5. The black trajectory show the current highest weight particle, and the positions of all the particle are marked with black dots. The colour correspond to the predicted magnetic field norm value, and the opacity is inversely proportional with the variance of the estimate.

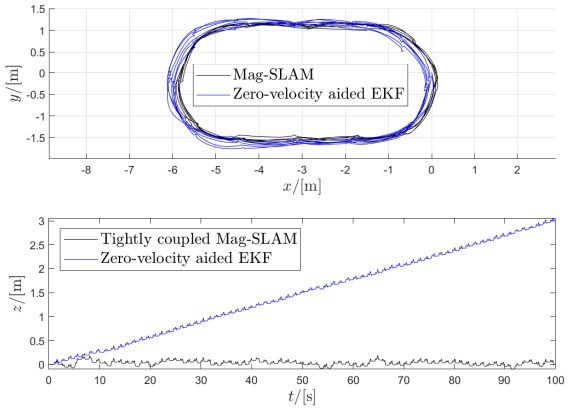

Fig. 6. Comparison of the position trajectories obtained from the ZUPT-aided EKF from [8] and the proposed Algorithm 1 for foot-mounted sensor. The top plot shows the error in the xy-plane, and the bottom plot shows the error along the z-dimension.

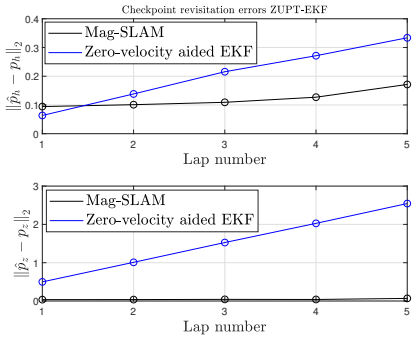

Fig. 7. The average checkpoint revisitation error for each of the five laps is plotted as a circle. Each blue line show the revisitation error of the ZUPT-aided EKF from [8] of one of the twelve checkpoints developing over time. Each black line shows the revisitation error of Algorithm 1 of one of the twelve checkpoints developing over time. The top plot shows the revisitation errors of the x and y-coordinates only, while the bottom plot compares the revisitation errors of the three dimensional position.

particles has a magnetic field state vector estimate $\widehat{m}_t^i$ that has dimension N_{m}, and a magnetic field state covariance P_m^i that has dimension $N_{\mathrm{m}} \times N_{\mathrm{m}}$. The number of required basis functions decreases when the length scale of the anomalies l_{SE} relative to the size of the domain Ω increases [14]. A way to reduce the number of necessary basis functions is, therefore, to use multiple tiles that each map a smaller domain. This method was implemented by [14], and the results they present indicate that executing the reduced-rank GP regression for magnetic field mapping in multiple tiles rather than a single domain covering all of the estimated positions is feasible.

Further research could be in the direction of making a map of all three magnetic field components instead of only the magnetic field norm. For the method to be useful in search and rescue scenarios, it could be useful to investigate if it can be made tolerant to changes in the magnetic field due to building collapse or extreme temperatures. Another possible direction is to investigate if maps from multiple sources could be fused to one map so that measurements from multiple people moving around in the same space could be used to improve on each other's estimates. A question that would have to be answered before the method could be used in practice is to investigate how different movement patterns can be taken into account, such as crawling, jumping, running or moving up or down an elevator.

REFERENCES

[1] V. Nunavath, A. Prinz, and T. Comes, "Identifying first responders information needs: Supporting search and rescue operations for fire emergency response," *International Journal of Information Systems for Crisis Response and Management*, vol. 8, pp. 25–46, Jan. 2016.

[2] L. Coyle, S. Neely, P. Nixon, and A. Quigley, "Sensor aggregation and integration in healthcare location based services," in *In proceedings of Pervasive Health Conference and Workshops*, pp. 1–4, Nov. 2006.

[3] H. Zhao, Z. Wang, Q. Gao, M. Hassan, and A. Alelaiwi, "Smooth estimation of human foot motion for zero-velocity-update-aided inertial pedestrian navigation system," *Sensor Review*, vol. 35, no. 4, pp. 389–400, 2015.

[4] O. J. Woodman, "An introduction to inertial navigation," tech. rep., Computer laboratory University of Cambridge, 2007.

[5] R. Harle, "A survey of indoor inertial positioning systems for pedestrians," *Communications Surveys and Tutorials, IEEE*, vol. 15, pp. 1281–1293, Jan. 2013.

[6] E. Foxlin, "Pedestrian tracking with shoe-mounted inertial sensors," *IEEE Computer Graphics and Applications*, vol. 25, pp. 38–46, Nov. 2005.

[7] M. Angermann, M. Frassl, M. Doniec, B. J. Julian, and P. Robertson, "Characterization of the indoor magnetic field for applications in localization and mapping," in *Proceedings of International Conference on Indoor Positioning and Indoor Navigation*, (Sydney, Australia), pp. 1–9, Nov 2012.

[8] I. Skog, "Openshoe matlab framework." `http://www.openshoe.org/?page_id=362`.

[9] J. Nilsson, I. Skog, P. Händel, and K. V. S. Hari, "Foot-mounted INS for everybody - an open-source embedded implementation," in *Proceedings of IEEE/ION Position, Location and Navigation Symposium*, (Myrtle Beach, SC, USA), pp. 140–145, April 2012.

[10] P. Robertson, M. Frassl, M. Angermann, M. Doniec, B. Julian, M. Puyol, M. Khider, M. Lichtenstern, and L. Bruno, "Simultaneous localization and mapping for pedestrians using distortions of the local magnetic field intensity in large indoor environments," in *Proceedings of International Conference on Indoor Positioning and Indoor Navigation*, (Montbeliard-Belfort, France), Oct. 2013.

[11] I. Vallivaara, J. Haverinen, A. Kemppainen, and J. Röning, "Magnetic field-based SLAM method for solving the localization problem in mobile robot floor-cleaning task," in *in Proceedings of IEEE 15th International Conference on Advanced Robotics: New Boundaries for Robotics*, (Tallin, Estonia), pp. 198–203, July 2011.

[12] C. E. Rasmussen and C. K. I. Williams, *Gaussian processes for machine learning*. MIT Press, 2006.

[13] A. Solin, M. Kok, N. Wahlström, T. B. Schön, and S. Särkkä, "Modeling and interpolation of the ambient magnetic field by Gaussian processes," *IEEE Transactions on Robotics*, vol. 34, pp. 1112–1127, Aug. 2018.

[14] M. Kok and A. Solin, "Scalable magnetic field slam in 3D using Gaussian process maps," in *Proceedings of the 20th International Conference on Information Fusion*, (Cambridge, UK), pp. 1353–1360, Jul. 2018.

[15] M. Kok and T. B. Schön, "Magnetometer calibration using inertial sensors," *IEEE Sensors Journal*, vol. 16, Jan. 2016. no 7.

[16] O. Egeland and J. Gravdahl, *Modeling and Simulation for Automatic Control*. Jan. 2002.

[17] I. Skog, J. Nilsson, and P. Händel, "Evaluation of zero-velocity detectors for foot-mounted inertial navigation systems," in *Proceedings of International Conference on Indoor Positioning and Indoor Navigation*, (Zürich, Switzerland), pp. 1–6, Sept. 2010.

[18] A. Solin and S. Särkkä, "Hilbert space methods for reduced-rank Gaussian process regression," *Statistics and Computing*, vol. 30, pp. 419–446, Jan. 2014.

[19] N. Wahlström, M. Kok, T. B. Schön, and F. Gustafsson, "Modeling magnetic fields using Gaussian processes," in *Proceedings of IEEE International Conference on Acoustics, Speech and Signal Processing*, (Vancouver, Canada), pp. 3522–3526, May 2013.

[20] C. Fischer, P. Sukumar, and M. Hazas, "Tutorial: Implementing a pedestrian tracker using inertial sensors," *Pervasive Computing, IEEE*, vol. 12, pp. 17–27, Apr. 2013.

[21] T. B. Schön, F. Gustafsson, and P.-J. Nordlund, "Marginalized particle filters for mixed linear/nonlinear state-space models," *IEEE Transactions on Signal Processing*, vol. 53, pp. 2279–2289, Jul. 2005.

[22] F. Gustafsson, "Statistical sensor fusion," 2013. Studentlitteratur AB.

[23] M. Kok, J. D. Hol, and T. B. Schön, "Using inertial sensors for position and orientation estimation," *Foundations and Trends in Signal Processing*, vol. 11, no. 1-2, 2017.

[24] J. Chung, M. Donahoe, C. Schmandt, I.-J. Kim, P. Razavi, and M. Wiseman, "Indoor location sensing using geo-magnetism," in *in Proceedings of the 9th International Conference on Mobile Systems*, pp. 141–154, Jan. 2011.

[25] M. Crombaghs, E. de Min, and G. van Hees, *The First Absolute Gravity Measurements in The Netherlands: Period 1991-1999*. Publications on geodesy, NCG, 2002.

[26] F. Gustafsson, F. Gunnarsson, N. Bergman, U. Forssell, J. Jansson, R. Karlsson, and P.-J. Nordlund, "Particle filters for positioning, navigation, and tracking," *IEEE Transactions on Signal Processing*, vol. 50, pp. 425–437, Mar. 2002.